Discrimination between drug-resistant and non-resistant human melanoma cell lines by FTIR spectroscopy

A. Zwielly,[a] J. Gopas,[bc] G. Brkic[b] and S. Mordechai*[a]

Received 28th March 2008, Accepted 23rd September 2008
First published as an Advance Article on the web 24th October 2008
DOI: 10.1039/b805223a

We investigated the ability of FTIR-microscopy to define spectral changes between drug-sensitive and drug-resistant human melanoma cells. As a model system, a resistant melanoma cell line (GAC) was selected with cisplatin from parental (GA) cells. Using Fourier transform infrared spectroscopy (FTIR) we investigated the ability to differentiate between the resistant variant derived from the sensitive parental cell line, in the absence of cisplatin. We determined and validated spectral parameters (biomarkers) that differentiated between the two cell lines. By applying the principal component analysis (PCA) model, we reduced the original data size to six principal components. We detected a significant and consistent increase in the cell's DNA/RNA ratio as well as an increase in the lipid/protein ratio in the resistant cells. These results strongly support the potential of developing FTIR microspectroscopy as a simple, reagent-free method for the identification of drug-resistant cells. Rapid detection of tumors resistant to a particular drug, should contribute to the ability of the physician to choose an effective treatment protocol.

Introduction

Melanoma is a malignant tumor of melanocytes which are found predominantly in skin. It is one of the rarer types of skin cancer but causes the majority of skin cancer related deaths. Despite many years of intensive laboratory and clinical research, the sole effective cure is surgical resection of the primary tumor before it metastasizes to other organs. Various chemotherapy agents are used to treat metastatic melanoma but the overall success in metastatic melanoma is quite limited, since this tumor type is usually intrinsically resistant to anti cancer drugs. The 5 year survival rate of patients with metastases to the subcutaneous and distant lymph nodes is less than 19%.[1] Chemotherapy further selects for tumor cells with "acquired" resistance. Thus, drug resistance is a major complication in cancer treatment and accounts for the failure of chemotherapy to cure the majority of patients. Drug resistance has been described as "the single most common reason for discontinuation of a drug".[2]

There is a need to develop new approaches that are safe, noninvasive, and effective to detect changes in premalignant cells and cells which develop resistance to different treatment modalities. One technique that emerged as a powerful tool for classification based on chemical analysis is the Fourier transform infrared (FTIR) microspectroscopy (MSP), due to its ability to provide detailed information on the spatial distribution of chemical composition at the molecular level.[3] Its applications cover a range of disciplines including material science,[4] forensics,[5] biochemistry,[6] biomedical science, and geochemistry,[7] comprising both basic and applied research goals. FTIR-MSP has shown encouraging trends in the field of drug resistance research in the last decade. Differences in the absorbance spectra in the mid-IR region reflect global biochemical modifications, and may be used to classify various cell types. Liu *et al.*[8] examined the IR spectral changes corresponding to lipid and nucleic acid and showed that they differ between drug resistant and drug sensitive leukemic cells. The general spectral alterations found in these cells were similar to those in multi-drug resistant K562 MDR cells.[9] Chekhun *et al.*[10] increased the sensitivity of IR and surface enhanced infrared absorption spectroscopy (SEIRA) of nucleic acids by using a gold substrate. They showed that DNA from resistant tumor cells has rigid structural features, while the DNA of sensitive cells is more flexible. Exposure to anticancer drugs drastically change the structure of the DNA helix. In addition, lipid molecular modifications were also detected after exposure to cisplatin, such as lipid pack chain disorder. and formation of phospholipids-cisplatin complexes.

Cell cultures have been the focus of many works using IR spectroscopy.[11–14] and monitoring by light microscopy.[15] In contrast to tissue biopsies, cell lines are homogenous, and it is possible to control cell culture parameters including cell division, apoptosis, malignant transformation and drug resistance. Their use is of invaluable help to dissect and define IR parameters of interest.

FTIR-MSP was used to examine cells resistant to cisplatin, a well known cytotoxic drug widely used against many tumors, including melanoma. Cellular resistance to this drug is multi factorial and consists of mechanisms that limit the formation of lethal platinum-DNA adducts and mechanisms that enable a cell to repair or tolerate platinum-DNA damage once it occurs. When cells become resistant to cisplatin, the doses must be increased; but a large dose escalation can lead to severe multi organ toxicities especially in kidneys and bone marrow, as well as intractable vomiting, and deafness.[16]

[a]*Department of Physics and the Cancer Research Center, Ben-Gurion University (BGU), Beer-Sheva, 84105, Israel. E-mail: shaulm@bgu.ac.il; Fax: +972-8-647 2903; Tel: +972-8-646 1749*
[b]*Department of Microbiology and Immunology, Faculty of Health Sciences, Ben Gurion University, Beer-Sheva, Israel*
[c]*Department of Oncology, Soroka University Medical Center, Beer-Sheva, Israel*

The ability to recognize efficiently drug resistant tumors to specific drugs could be of great benefit to determine the choice of chemotherapy with the highest probability of success and to monitor the emergence of drug resistant tumor cells after treatment. Melanoma cells are intrinsically resistant to many drugs. In addition, even more resistant variants arise following "natural selection" due to chemotherapy. Therefore, it is of importance to identify and classify spectral patterns of a variety of melanoma cells, reflecting subtle changes difficult to detect by vibrational spectroscopy methods.

Materials and methods

Cell lines

The GA parental cell line, was established from a metastatic explant of a melanoma patient. The cells were maintained in DMEM medium supplemented with 5% L-glutamine, 5% antibiotics (streptomycin and penicillin) and 10% fetal calf serum (Biological Industries, Kibbutz Beit Haemek, Israel) and regularly propagated by trypsinization. Cisplatin resistant GA cells (GAC) were obtained by a single step selection protocol, as reported earlier.[17] Briefly: 10^6 GA cells were treated with the LD_{90} concentration of cisplatin for five days. The cells were washed with PBS and allowed to propagate and stabilize in fresh medium. The drug-selected cells were isolated and tested for resistance to cisplatin by determining the LD_{50} cytotoxic concentration of cisplatin. The LD_{50} of GAC cells after 48 hours incubation with the drug was 65 μM, as compared to 20 μM, the LD_{50} of GA cells.[18] Thus, GAC cells are 3.25 more resistant to cisplatin than GA cells. GA and GAC cells are morphologically indistinguishable. Resistant GAC cells were grown for several weeks in the absence of cisplatin before preparation for FTIR measurements. Previous to FTIR analysis, the sensitive or resistant phenotype of the cells was confirmed by the cytotoxic assay. All measurements were done in the absence of cisplatin on cells from independent cultures over a period of several months.

Sample preparation for Fourier transform infrared microscopy measurements

Since ordinary glass slides exhibit strong absorption in the wavelength range of interest, zinc sellenide crystals, which are highly transparent to IR radiation, were used. Cell cultures were washed with a physiological saline solution and harvested from the tissue culture plates after treatment with trypsin (0.25%) for 2 min. The cells were washed three times with saline and resuspended at a concentration of 10^6 cells/ml. 5 μl drops of each sample containing 5000 cells, were placed on the zinc sellenide crystal and air dried for 1 h. The dried drops typically produced a 1 mm radius monolayer-cell of 10 μm thickness.

Fourier transform infrared microspectroscopy and data acquisition

FTIR measurements of dried cells were performed using the FTIR microscope IR scope 2 with a liquid-nitrogen-cooled mercury-cadmium-telluride (MCT) detector, coupled to the FTIR spectrometer (Bruker Equinox model 55/S, OPUS software). To achieve a high signal-to-noise ratio (SNR), 128 co-added scans were collected in each measurement in the wavenumber region 800 to 4000 cm^{-1}. The measurement site was circular with a diameter of 100 μm and spectral resolution of 4 cm^{-1} was used. To reduce cell amount variation and guarantee proper comparison between different samples, the following procedures were adopted:

1. Each sample was measured at least five times at different spots.

2. ADC (analog to digital converter) rates were empirically chosen between 1000 to 1200 counts/sec (which allows us to measure microscopic spots with similar cellular density).

3. The obtained spectra were baseline corrected using the rubberband method with 64 consecutive points and normalized using *min–max normalization* in OPUS software.[19] Vector normalization for the entire spectra have also been tested and gave negligible changes in the results.

Statistical analysis

Data reduction by principal component analysis (PCA) was implemented. Mean centering was applied to the entire dataset before PCA.[20] All spectra were treated by our computer code built on the MatLab[21] application. This code is based on the iterative NIPALS algorithm. Loadings were computed by manipulation on the calculated scores matrix[22] and were taken with absolute values. The obtained data points represented by the calculated PCs were used to distinguish between the two cell types. Significance of the results was determined by the unpaired t-test included in the *Origin* software.[23] Differences were considered significant at $P < 0.05$.

Results

Spectral differences between cisplatin-sensitive and resistant cells

Untreated (a) and cisplatin-treated (b) GA cells are shown in Fig. 1. As can be seen in Fig. 1b apoptosis is induced in cells incubated with cisplatin. We analyzed the FTIR spectra of 50 different samples of parental GA cells and 48 samples of their

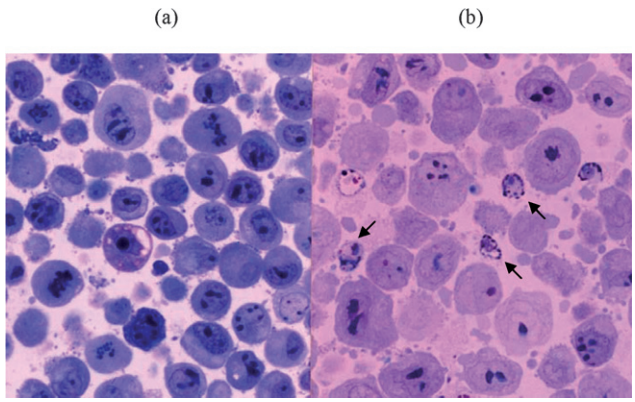

Fig. 1 Semi-thin sections of GA cells untreated (a) and treated with cisplatin (b). Cisplatin treated (20 mM for 48 hours) and untreated cells were fixed with glutaraldehyde and blocks for electron microscopy were prepared. 1 μm sections were cut and laid on glass slides. The sections were stained with methylene blue, azure II and basic fuccin. Arrows point towards apoptotic cells (b). 600×.

cisplatin resistant GAC cells. The spectra were obtained on cells in the absence of cisplatin. Changes between the two groups were noticed in most constituents of the cells including proteins, lipids, polysaccharide and amino acids, but only few biomarkers were found statistically significant.

The 2980–3000 cm^{-1} spectral region

One region with significant and consistent differences was identified at 3000 to 2820 cm^{-1}. For an effective comparison, the examined regions were isolated from the entire spectra, normalized to the CH_2 antisymmetric band (~2920 cm^{-1}), which has the maximum absorbance in this region. and baseline corrected. The results (Fig. 2) show four prominent absorbance bands: near 2852 cm^{-1}, due to the symmetric stretching of the methylene chains in membrane lipids; at 2871 cm^{-1}, arising from the symmetric CH_3 (methyl) stretching; at 2923 cm^{-1}, due to the antisymmetric CH_2 stretch; and at 2958 cm^{-1} due to antisymmetric stretching of the methyl groups of both lipids and proteins. It is shown in Fig. 2 that the average absorption intensities of GA and GAC cells are distinctive at 2852 cm^{-1} and 2958 cm^{-1} bands. It was found that the best discriminating values were obtained by deriving the intensity ratio of these two vibrational modes (i.e., A(2958)/A(2852) or ν_{as} CH_3/ν_s CH_2). The dimensionless ratio eliminates a possible artifact, which may arise due to the baseline contribution underneath each band.

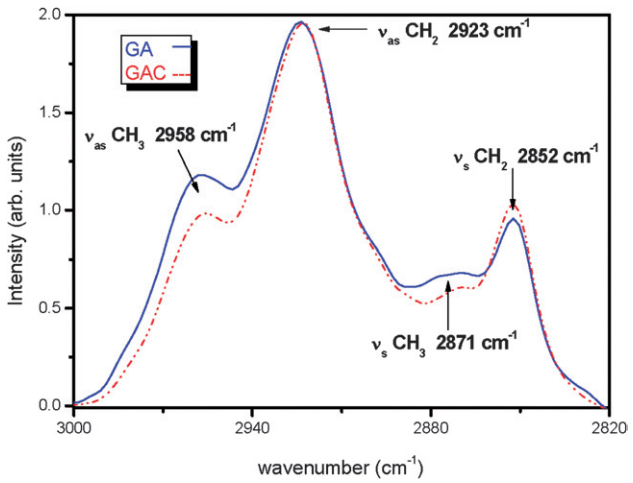

Fig. 2 Averaged FTIR spectra in the regions 2820–3000 cm^{-1} of resistive (GAC) and non-resistive (GA) cells.

Table 1 Statistical analysis of the biomarkers derived from the FTIR spectra of GA and GAC melanoma cells

	A_{2958}/A_{2852}		A_{1121}/A_{1022}		A_{1740}/A_{1400}	
	GA	GA cis	GA	GA cis	GA	GA cis
Mean	1.26	1.16	1.23	2.01	0.16	0.29
SD	0.08	0.11	0.43	0.82	0.09	0.03
Max value	1.40	1.29	2.07	3.09	0.37	1.40
Min value	1.05	0.87	0.56	0.40	0.06	0.21
T-value	4.493		5.837		8.314	
P-value	1.95×10^{-5}		7.52×10^{-8}		6.9×10^{-13}	

Table 1 summarizes the statistical values of this ratio for the resistant and parental cell line. The *t*-value of the two groups is 4.49 and the *p*-value is 1.95×10^{-5}. Therefore, this ratio may be considered as a satisfactory biomarker for the distinction of the transformation towards drug resistance.

The 1200–1800 cm^{-1} spectral region

An absorbance bands in the region 1200–1800 cm^{-1} (data not shown) was normalized to the amide I (~1650 cm^{-1}). The region from 1500–1800 cm^{-1} is almost solely subjugated to the conformation-sensitive amide I and amide II bands, which are the most dominant bands in the spectra of nearly all complex biological systems. Another important biomarker can also be obtained from the shoulder near 1740 cm^{-1}, resulting primarily from C=O stretching vibrations of the ester functional groups in phospholipids.[24] The lipids in the membrane are composed mainly of phospholipids that determine membrane structure, stability, fluidity and membrane enzymatic activity. Thus, monitoring lipid absorbance of resistant cells is an important diagnostic parameter which can be associated with the drug resistance mechanism. Substantial differences were identified at 1740 cm^{-1} (C=O bonds of lipids), which express increasing intensity in GAC cells. This result cross-validates the differences observed between the cells in the 2800–3000 cm^{-1} region, since the ~2852 cm^{-1} band, mainly due to lipid content, shows the same trend as the 1740 cm^{-1} band. The lipid-protein ratios were calculated using the intensities at 1740 and 1400 cm^{-1}.[25] This quantitative spectral analysis shows a significant increase in the lipid contribution of GAC over GA. Thus a significant increase in the lipid-protein ratio in the GAC cells is expected (Table 1).

The 1000–1200 cm^{-1} spectral region

The 1145 to 1000 cm^{-1} region shown in Fig. 3 contains many overlapping vibrational modes associated with absorbance of macromolecules such as proteins, nucleic acids, carbohydrates, and phospholipids. The bands at 1083 and 1056 cm^{-1} correspond to absorbance of the ν_s PO_2^- of phosphodiesters of nucleic acids[3] and the O–H stretching coupled with C–O bending of C–OH groups of carbohydrates, respectively.[19] Additional bands at 1121 and 1022 cm^{-1} can be clearly seen in the second derivative spectra [Fig. 3(b)]. Previous works have shown that the band at 1121 cm^{-1} arises from RNA absorbance, whereas the 1022 cm^{-1} shoulder is due to DNA.[26–28] The ratio between these two bands A(1121)/A(1022) ratio (assigned as RNA/DNA), is an additional statistically significant spectral biomarker. Although the variability of this biomarker is high due to overlapping absorbance, the average values measured are still statistically significant (Table 1).

PCA analysis

The main objective of this research is to identify and validate spectral differences in FTIR microscopy between GA, a human melanoma cell line and its cisplatin resistant variant, GAC. We measured the spectra which include 512 vector components corresponding to the absorbance intensity in each scanned wavenumber. These results were obtained after excluding the 1800–2820 cm^{-1} uninformative region ncompassing the

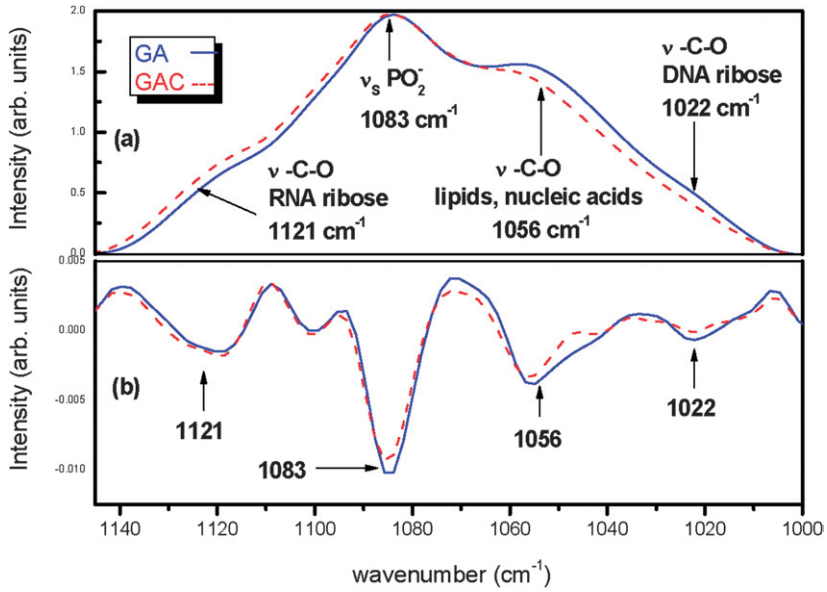

Fig. 3 (a) Averaged FTIR spectra in the regions 1000–1145 cm^{-1}. (b) The second derivative spectra at this region of resistant (GAC) and non-resistant (GA) cells.

atmospheric CO_2 absorption band. In order to reduce the number of variables, the PCA procedure has been implemented. The PCA analysis reduces the number of variables to six principal component that identify 98.4% of the variety in the data. It is often mistakenly assumed that the higher the variety percentage described by PCA, the more realistic is the description of the data. On the contrary, the variety percentage described by PCA should be proportional to the expected error, thus reducing the built-in errors in the data. The PCA model enables presentation of the data in six dimensions, which cannot be presented graphically. Nonetheless, presentation of two or three PCs is possible and allows the distinction between the two cell types. The scores of PC1 vs. PC3 and PC4 vs. PC3 of the entire dataset are presented in Fig. 4(a) and Fig. 4(b) respectively. As can be seen, excellent differentiation between the two cell types can be achieved by comparing PC1 with PC3 [Fig. 4(a)]. The addition of a third component, PC4 in Fig. 4(a) contributes to obtain a better separation between the cells (data not shown). In contrast, other PCs pairs or groups of three PCs were found not informative. The data is summarized in Table 2.

As shown in Fig. 4(a), the PC1 vs. PC3 plane, good distinction between the two groups was attained using the line described as: $PC1 = 15.12 \times PC3 + 2.20$. It was calculated that the angle of this line is almost perpendicular to the PC3 axis (86.2°). Therefore the major separation between the two groups is derived from the PC3 axis. PC3 includes only 2 percent of the data variation. In order to identify which significant biomarkers are represented in such a small variation we concentrated on the absolute value of the PC3 loadings [Fig. 5(a)]. In contrast to the PC3 axis, which corresponds to the changes between GA and GAC, the PC1 axis, represents 89 percent of the variety in the data, reflecting mainly the individual diversity within each cell type in the sample [Fig. 5(b)]. One of the purposes of this research was to eliminate the individual diversity between the cells as classifying generator between the resistant and sensitive cells. In order to better define the changes due to a possible increase in the natural diversity of the cells within each group, two subgroups of cells from each cell line were studied. These subgroups originated from cell aliquots frozen and then thawed at different times to continue to be carried in cell culture. After several generations in cell culture cells may diverge from the original cell line. Changes due to "natural" divergence were largely cancelled out by comparing measurements within the subgroups. The distinction based on the same biomarker, drastically reduced the possibility that the changes observed between GA and GAC cells were due to natural diversity. The specific bands of PC3 spectra [Fig. 5(a)], also benefit from reduced spectral congestion allow better resolution than the broad contour of PC1 spectra [Fig. 5(b)]. The 2958 and 2852 cm^{-1} most prominent PC3 loadings bands were mostly absent in the PC1 loadings. As mentioned earlier these biomarkers represent the methyl and methylene membrane lipid components. Another prominent PC3 loadings peak at 1740 cm^{-1} represents lipid content and can differentiate between the cells. This peak is almost absent in PC1. Other bands with less differential intensity between the two loadings are the 1670 cm^{-1} (Amide I, β-turns of proteins) and 1560 cm^{-1} (Amide II). The 1400 cm^{-1} corresponds to the C═O symmetric stretch of the COO, C-terminus end of proteins. This peak shows the reverse trend, higher in PC1 than PC3 intensity. The inset in Fig. 5 represents the extended 1000–1180 cm^{-1} region of PC3 loadings. Five prominent peaks appear in this spectral region; 1022, 1083 and 1121 cm^{-1}, representing the nucleic acids phosphodiester bonds of DNA and RNA respectively. The peak at 1050 cm^{-1} can be assigned to either lipid or carbohydrate vibrational modes and the 1072 cm^{-1} peak corresponds to carbohydrates.

The prominence of the PC3 methyl and methylene region (2800–3000 cm^{-1}) over PC1 (Fig. 5), prompted us to estimate the contribution of this region to the overall differentiation between the cells. Integration over this region showed that the mean absorbance was reduced in the resistant GAC cells. Highly

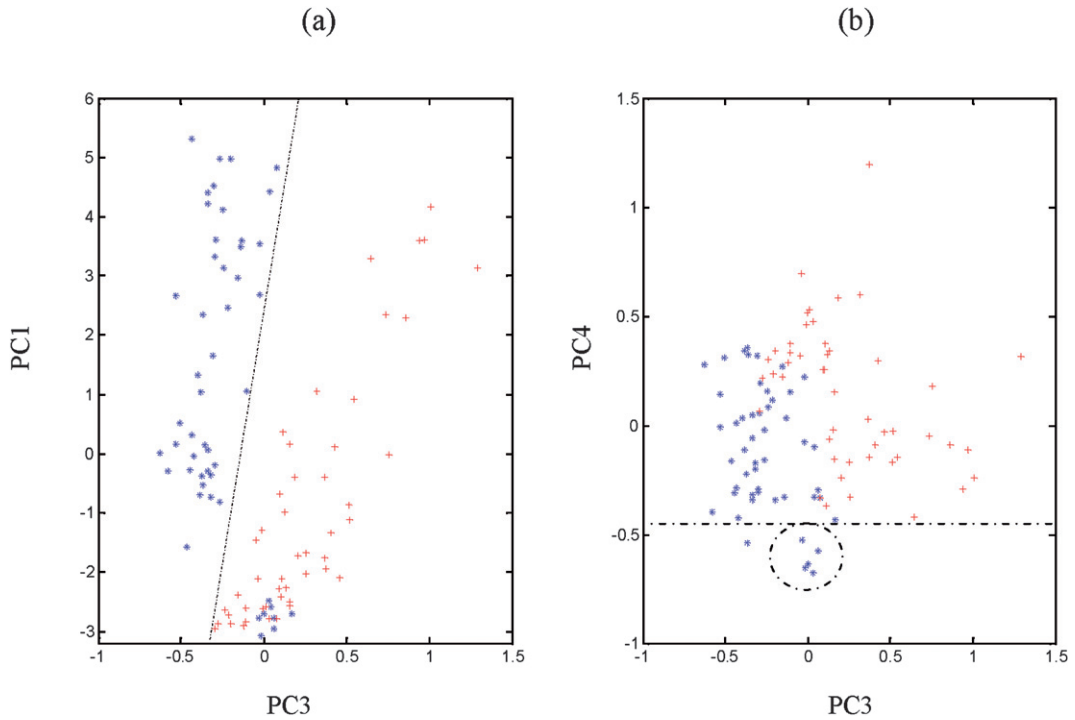

Fig. 4 Principle component analysis (PCA) model employed on the data reducing the 512 valid measured variables in the spectra to 6 PCs, which describe 98.4% of the data variance. (a) Good distinction between resistant (red +) and non-resistant (blue *) cells has been achieved using PC1 vs. PC3. (b) PC4 vs. PC3 resolved some of the data points (circled) indicating a better distinction between the two groups after adding PC4 to create 3D separation.

Table 2 Success rates in identification of sensitive (GA) and resistant (GAC) cells using 2D and 3D PCA model (PC1 vs. PC3 and PC1 vs. PC3 vs. PC4 respectively) and the methyl-methylene region vs. amide I

Cell type	CH_2 & CH_3 vs. Amide I	2D PCA model	3D PCA model
Sensitive	41/50	42/50	47/50
(GA)	82%	84%	93%
Resistant	40/48	48/48	48/48
(GAC)	83%	100%	100%
Total	81/98	90/98	93/98
positive	82%	91%	95%

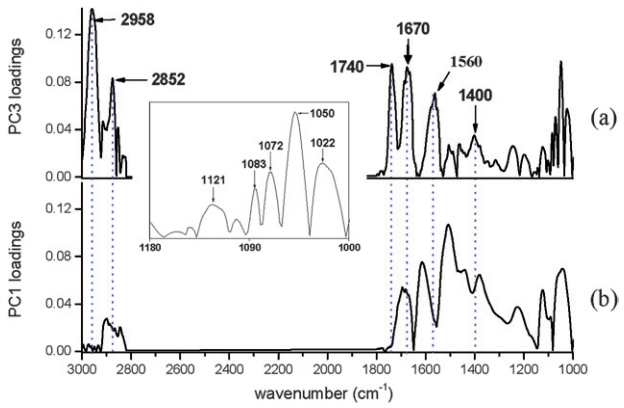

Fig. 5 Absolute value loadings of (a) PC3, (b) PC1. The inset displays the expanded region 1000–1180 cm^{-1} of PC3.

significant t-test results with a p-value of 6.49×10^{-11} and a t-value of 7.37 were obtained. Another region of biochemical interest is the protein region. Integration over the amide I region 1630–1700 cm^{-1} also showed high significance ($p \leq 1.43 \times 10^{-6}$, $t \geq 5.15$) with an increased mean integrated absorbance in GAC cells. Fig. 6 shows the summed methyl and methylene groups versus Amide I. Two Gaussian distributions are clearly observed for GA and GAC with a substantial differentiation attained between the two groups (Table 2).

Discussion

In the present work we conducted a comparative study between a cisplatin-sensitive melanoma cell line and its selected, cisplatin-resistant variant. The main goal of this work was to determine whether FITR spectra could differentiate between morphologically undistinguishable cells differing only in their sensitivity to a common chemotherapeutic drug. The ability to develop such a diagnostic tool will contribute to the selection of better and more efficient chemotherapy.

We have traced a significant increase in the methylene/methyl CH_2/CH_3 ratio (2820–3000 cm^{-1} region) in GAC, as compared to GA cells (Table 1). Since proteins contain, on the average, an equal amount of methyl and methylene groups, a protein change alone would have modified both the CH_3 as well as the CH_2 stretching to the same extent, therefore the difference in the spectra are most likely related to an increase of fatty acids and phospholipids rather than to the protein content. Gaigneaux *et al.*[9] and Le Moyec *et al.*[29] obtained opposite results when multidrug resistant K562 cells and their sensitive parental cells

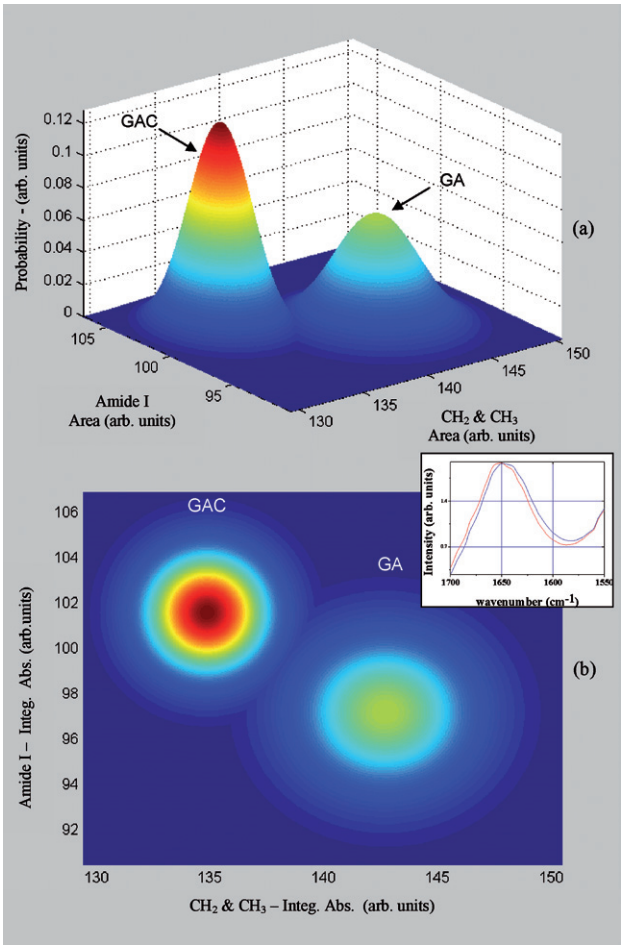

Fig. 6 (a) Gaussian distribution of the absorbance intensity of methyl and methylene integrated region 2800–3000 cm^{-1} versus Amide I. (b) Gaussian top view showing good differentiation between the two groups based on the methyl and methylene integrated region. The upper right inset shows the averaged amide I spectral region of GA (blue) and GAC (red).

were tested. These authors observed a decrease in the methylene/methyl CH_2/CH_3 ratio of the resistant cells in the presence of donorubicin and taxol. Nonetheless, when the resistant K562 cells were incubated for several passages in the absence of the drugs, Le Moyec *et al.*[29] obtained the reverse spectra, similar to the spectra measured in GAC cells in the absence of cisplatin. Cisplatin-sensitive neuroblastoma cells, in the presence of the drug, showed an increase in the methtl/methylene ratio in comparison to untreated cells. The methyl/methylene ratio was unchanged in the resistant cells in the presence or absence of cisplatin.[30] Thus, stress induced by a variety of cytotoxic drugs induce similar spectral changes of this kind.

Several mechanisms of resistance to cisplatin have been described, including decreased membrane transport of the drug, increased cytoplasmic detoxification, DNA repair, and tolerance to DNA damage.[31] Cisplatin is highly polar and enters cells relatively slowly in comparison to other classes of small-molecule cancer drugs. The uptake of cisplatin is influenced by factors such as sodium and potassium ion concentrations, pH and the presence of reducing agents. A role for transporters or gated channels has been postulated in addition to passive diffusion.[32]

In contrast to the mechanism of multi-drug resistance (MDR) to mainly natural-product-based drugs, which is caused by the overexpression of ATP-dependent efflux pumps such as P-glycoprotein—it is generally decreased uptake, rather than increased efflux that predominates in platinum-drug resistance.[32] It is therefore possible that an increase in membrane lipid content as observed in GAC cells may result in membrane fluidity changes which, could diminish cisplatin diffusion into the cell. In the past few years, active uptake of cisplatin has been recognized. The major plasma-membrane transporter involved in copper homeostasis, copper transporter-1 (CTR1), has been shown to have a substantial role in cisplatin influx.[33,34] Its inhibition results in 2–3 fold increase in cisplatin drug resistance. Conceivably, inhibition of cisplatin active uptake may be also due to modifications in secondary and tertiary protein conformation. The amide I region differences between the cells show structural protein modifications which are consistent with the results showed in Fig. 6. The 1695 cm^{-1} region (peptide bonds), 1685 cm^{-1} (antiparallel β-pleated sheets), 1675 cm^{-1} (β-turns of proteins), 1655 cm^{-1} (α-helical structures) show higher absorption intensity in GAC cells. In contrast, the 1637 cm^{-1}, β-pleated sheet structure bands is decreased in these cells.

A highly significant cross validation of the CH_2/CH_3 findings was obtained using the total lipid/protein ratio as represented by the 1740/1400 cm^{-1} ratio (Table 1). The same trend observed in the methylene/methyl ratio is seen. Differences between the cells in the 1050 cm^{-1} peak obtained in the PC3 loadings (Fig. 5 inset) could be another complementary differential biomarker based on lipid membrane modifications between the cells. This biomarker is attributed mainly to the C=O ester functional groups in phospholipids.

Once inside the cell, cisplatin interacts preferentially with RNA and DNA. The interaction of cisplatin with RNA is limited, since a single damaged RNA molecule can be replaced by newly synthesized material; studies have revealed that cisplatin does not affect RNA synthesis, but that it tampers DNA synthesis. Moreover, when lethal doses of cisplatin were administered *in vitro* to cancer cells, only a small fraction, 1%–10% of RNA molecules were damaged.[35] Previous research on GA/GAC cells revealed distinctive mRNA molecules in the resistant cells[36] as well as a distinctive DNA signature in GA cells in comparison to GA drug resistant variants.[17] Interaction of cisplatin with DNA occurs mainly through nitrogen atoms of the DNA base pairs, specifically, N_7 of purines, specially guanine. N_7 is free to bind cisplatin because it does not form hydrogen bonds with any of the other DNA bases. Few changes in RNA and substantial changes in DNA were observed in our cells as a significant high ratio of A(1121)/A(1022) (Table 1) and as a strong intensity at 1022 cm^{-1} over the 1121 cm^{-1} wavenumber (Fig. 5), Our findings are in agreement with Gaigneaux *et al.*[9] although the DNA/RNA ratio in this work was not statistically significant.

To reduce the number of variables and to be able to classify two cells lines, we used PCA analysis. We found that the best separation is attained using two principal components, PC1 vs. PC3 with ~ 91 percents true identification [Fig. 4(a)]. Adding PC4 to the other two PCs increased this ratio to almost 96 percent. A distinction based on the methyl methylene versus amide I regions showed significant results (Table 2). The methyl

methylene region is a good classifying biomarker in our experimental model and it would be of interest to examine its significance in other cellular drug resistance models. This high rate of distinction success is in agreement with the results of other research on drug resistance cell-lines. Krishna *et al.*[37] achieved a full classification between MES-SA and Graf cells based on PC1 vs. PC2 analysis. Gaigneaux *et al.*[9] classified sensitive and multidrug resistant K562 cells with an accuracy of 93 percent using PCA combining with LDA analysis. FTIR measurements on ex-vivo isolated leukemic cells[8] predicted a sensitivity rate to chlorambucil and 2-chlorodeoxyadenosine of 85.7% and 80.3% respectively.

Natural cell diversity may exist in each cell line. PC1 represents this natural diversity encompassing most of the variety in the data (~89%) [Fig. 4(a)]. Natural variation is higher in GAC cells than in GA cells. Higher natural diversity in GAC cells may reflect more genetic instability, thus the ability to generate efficiently drug resistant variants.[17] In spite of the above, the differences between the two cell lines are mostly defined by PC3. PC3 represents a very small portion of the variety in the data (~2%). Thus, changes due to natural diversity in both cell lines are much more substantial than those caused by drug selection of parental GA cells. However these changes are random and are unable to distinguish between the two cell types. Therefore, in order to resolve between the two cell lines PC3 and not PC1 provides a meaningful distinction.

Conclusions

In conclusion, we show here that FTIR microscopy can differentiate between parental melanoma cells and their cisplatin drug resistant variant. Since melanoma is considered as an intrinsically drug resistant tumor, the ability to detect resistant variants above its innate resistance may be of importance. We also demonstrate that FTIR is a powerful tool for defining wide biochemical modifications in the cisplatin, non-MDR phenotype.

Acknowledgements

We gratefully acknowledge support by the Israel Science Fundation ISF 788/01, The Israel Ministry of Absorption through Science, The Richard H Holzer Fundation, The Samuel Goldstein Memorial Fundation, The Brener Family Fundation and The Prof. Lucia Pinczewska Gliksman Cancer Foundation.

References

1 C. M. Balch, A. C. Buzaid, S. J. Soong, M. B. Atkins, N. Cascinelli, D. G. Coit, I. D. Fleming, J. E Gershenwald, A. H. Jr, J. M. Kirkwood, K. M. McMasters, M. F. Mihm, D. L. Morton, D. S. Reintgen, M. I. Ross, A. Sober, J. A. Thompson and J. F. Thompson, *J. Clin. Oncol.*, 2001, **19**, 3635–3648.
2 D. B. Zamble and S. J. Lippard, *Trends in Biochemical Sciences*, 1995, **20**, 435–439.
3 J. Liquier and E. Taillandier, In *Infrared Spectroscopy of Biomolecules*, (ed. by H. H. Mantsch & D. Chapman). Wiley-Liss, John Wiley & Sons, INC., Publication, NY, 1996, pp. 131–158.
4 G. Bhagavannarayana, R. V. Ananthamurthy, G. C. Budakoti, B. Kumar and K. S. Bartwal, *J. Appl. Crystallogr.*, 2005, **38**, 768–771.
5 N. J. Crane, E. G. Bartick, R. S. Perlman and S. Huffman, *Journal of Forensic Sciences*, 2007, **52**(1), 48–53.
6 R. K. Sahu, S. Argov, A. Salman, U. Zelig, M. Huleihel, N. Grossman, J. Gopas, I. Kapelushnik and S. Mordechai, *J. Biomedical Optics*, 2005, **10**, 54017–54027.
7 J. Ramesh, A. Salman, Z. Hammody, B. Cohen, J. Gopas, N. Grossman and S. Mordechai, *J. Biochem. Biophys. Methods*, 2001, **50**, 33–42.
8 K.-Z. Liu, M. Xu1 and D. A. Scott, *British Journal of Haematology*, 2007, **136**, 713–722.
9 A. Gaigneaux, J.-M. Ruysschaert and E. Goormaghtigh, *Eur. J. Biochem.*, 2002, **269**, 1968–1973.
10 V. F. Chekhun, G. I. Solyanik, G. I. Kulik, V. P. Tryndiak, I. N. Todor, G. I. Dovbeshko and O. P. Repnytska, *Exp Clin Cancer Res.*, 2002, **21**(4), 599–607.
11 M. German, A. Hammiche, N. Ragavan, M. J. Tobin, J. L. Cooper, S. S. Matanhelia, A. C. Hindley, C. M. Nicholson, N. J. Fullwood, H. M. Pollock and F. L. Martin, *Biophys. J.*, 2006, **90**(10), 3783–3795.
12 Y. Yang, J. Sule-Suso, G. D. Sockalingum, G. Kegelaer, M. Manfait and A. El Haj, *Biopolymers*, 2005, **78**(6), 311–317.
13 L. Zhang, G. W. Small, A. S. Haka, L. H. Kidder and E. N. Lewis, *Appl. Spectrosc.*, 2003, **57**(1), 14–22.
14 J. Sule-Suso, A. Forster, V. Zholobenko, N. Stone and A. El Haj, *Appl. Spectrosc.*, 2004, **58**(1), 61–67.
15 C. Krafft, R. Salzer, S. Seitz, C. Ern and M. Schieker, *Analyst*, 2007, **132**, 647–653.
16 G. Chu, *Journal of Biological Chemistry*, 1994, **269**, 787–790.
17 G. Brkic, J. Gopas, N. Tanic, N. Dedovic-Tanik, D. Benharroch, E. Finkelstein-Jaworowsky and B. Dimitrijevic, *Anticancer Research*, 2003, **23**, 2601–2607.
18 M. D. Jonston, E. R. Fint and P. A. Young, *Methods in Enzymology*, 1981, **78**, 394–399.
19 S. Wartewig, *IR and Raman Spectroscopy*, John Wiley and Sons, Publication, NY, 2003, pp. 75–122.
20 K. R. Beebe, R. J. Pell, M. B. Seasholts, *Chemometrix*, Wiley 1998, pp. 48, 89.
21 MATLAB, Version 7.0, The MatWorks Inc. Natick, MA, 1999.
22 M. Diem, P. R. Griffith, J. M. Chalmers, *Vibrational Spectroscopy for Medical Diagnosis*, Wiley 2008, p. 40.
23 Origin Corporation (2002).
24 M. Diem, S. Boydston-White and L. Chiriboga, *Appl. Spectrosc.*, 1999, **53**, 148A–161A.
25 J. R. Mourant, Y. R. Yamada, S. Carpenter, L. R. Dominique and J. P. Freyer, *Biophys. J.*, 2003, **85**(3), 1938–47.
26 F. S. Parker, *Application of Infrared Spectroscopy in Biochemistry, Biology and Medicine*, Plenum Press, Publication, NY, 1971, pp. 477–491.
27 D. Naumann, *Appl. Spectrosc. Rev.*, 2001, **36**, 239–298.
28 E. Benedetti, E. Bramanti, F. Papineschi, I. Rossi and E. Benedetti, *Appl. Spectrosc.*, 1997, **51**, 792–797.
29 L. L. Moyec, R. Tatoud, A. Degeorges, C. Calabresse, Bauza, M. Eugene and F. Calvo, *Cancer Research*, 1996, **56**, 3461–3467.
30 M. Lindskog, C. Spenger, J. Jarvet, A. Gräslund and P. Kogner, *J. Natl. Cancer Inst.*, 2004, **96**, 1457–66.
31 L. Kelland, *Nature Reviews Cancer*, 2007, **7**, 573–584.
32 D. P. Gately and S. B. Howell, *Br. J. Cancer*, 1993, **67**, 1171–1176.
33 S. Ishida, J. Lee, D. J. Thiele and I. Herskowitz, *Proc. Natl. Acad. Sci. U. S. A.*, 2002, **99**, 14298–14302.
34 K. Katano, A. Kondo, R. Safaei, A. Holzer, G. Samimi, M. Mishima, Y.-M. Kuo, M. Rochdi and S. B. Howell, *Cancer Res.*, 2002, **62**, 6559–6565.
35 P. Pil, S. J. Lippard, In *Encyclopedia of Cancer*, J. R. Bertino, Ed. Academic Press:San Diego, CA, Vol. 1, 1997, pp. 392–410.
36 N. Tanic, G. Brkic, B. Dimitrijevic, N. Dedovic-Tanic, N. Gefen, D. Benharroch and J. Gopas, *Anticancer Research*, 2006, **26**, 2137–2142.
37 C. M. Krishna, G. Kegelaer, I. Adt, S. Rubin, V. B. Karth, M. Manfait and G. D. Sockalingum, *Biochem. et Biophys.*, 2005, **1726**, 160–167.

